PALEOCLIMATE

Glacial to Holocene changes in trans-Atlantic Saharan dust transport and dust-climate feedbacks

Ross H. Williams,[1]* David McGee,[1†] Christopher W. Kinsley,[1,2] David A. Ridley,[3] Shineng Hu,[4] Alexey Fedorov,[4] Irit Tal,[1] Richard W. Murray,[5] Peter B. deMenocal[6,7]

Saharan mineral dust exported over the tropical North Atlantic is thought to have significant impacts on regional climate and ecosystems, but limited data exist documenting past changes in long-range dust transport. This data gap limits investigations of the role of Saharan dust in past climate change, in particular during the mid-Holocene, when climate models consistently underestimate the intensification of the West African monsoon documented by paleorecords. We present reconstructions of African dust deposition in sediments from the Bahamas and the tropical North Atlantic spanning the last 23,000 years. Both sites show early and mid-Holocene dust fluxes 40 to 50% lower than recent values and maximum dust fluxes during the deglaciation, demonstrating agreement with records from the northwest African margin. These quantitative estimates of trans-Atlantic dust transport offer important constraints on past changes in dust-related radiative and biogeochemical impacts. Using idealized climate model experiments to investigate the response to reductions in Saharan dust's radiative forcing over the tropical North Atlantic, we find that small (0.15°C) dust-related increases in regional sea surface temperatures are sufficient to cause significant northward shifts in the Atlantic Intertropical Convergence Zone, increased precipitation in the western Sahel and Sahara, and reductions in easterly and northeasterly winds over dust source regions. Our results suggest that the amplifying feedback of dust on sea surface temperatures and regional climate may be significant and that accurate simulation of dust's radiative effects is likely essential to improving model representations of past and future precipitation variations in North Africa.

INTRODUCTION

North Africa exports hundreds of teragrams of windblown mineral aerosol over the tropical North Atlantic (TNA) each year (Fig. 1) (*1*, *2*), with significant climate and biogeochemical impacts. Dust's direct radiative effects result in scattering of incoming sunlight, reducing incident radiation and leading to a mean annual surface radiative impact estimated at −7.4 ± 1.5 W/m^2 over the TNA (*3*). Dust also reduces mid-tropospheric specific humidity (*4*) and increases stratocumulus cloud cover over the TNA (*5*, *6*), both of which provide additional negative radiative forcing. The resulting reduction in TNA sea surface temperatures (SSTs) due to dust loading has potentially important impacts on atmospheric circulation and precipitation patterns in both the TNA and West Africa (*7*–*9*) that may serve to amplify changes in the West African monsoon (*8*). In addition to its radiative effects, dust supports high rates of nitrogen fixation in the TNA by supplying iron to surface waters (*10*), and it is a primary source of nutrients to soils in the western Atlantic and tropical South America (*11*–*13*).

Sediment records from the northwest African margin display high-amplitude changes in African dust deposition on orbital and millennial time scales (Fig. 2B), suggesting that dust may have played an important role in past climate and ecosystem changes in the region. Over the last 20,000 years (ky), maximum dust fluxes were associated with reduced North Atlantic SSTs during Heinrich Stadial 1 (HS1) and the Younger Dryas (YD), reaching levels at least a factor of 2 higher than mean fluxes over the last 2 ky (*14*, *15*). In the early Holocene, dust fluxes were lower by factors of 2 to 5 than during the last 2 ky throughout the precessionally forced African Humid Period [AHP; 11,700 to 5000 years ago (ka)] (*14*, *15*). Dust deposition along the African margin rose abruptly at the end of the AHP at approximately 5 ka (*15*, *16*), suggesting a change more rapid than insolation forcing superimposed on a multimillennial reduction in monsoon strength (*17*). Dust fluxes then gradually increased throughout the last 4 ky in parallel with declining summer insolation. Lake-level records (*18*), river discharge reconstructions (*19*), hydrogen isotopic values from plant wax biomarker compounds (*17*), and other proxy data indicate terrestrial paleohydrological shifts during the AHP that are consistent with dust flux records.

These substantial changes in dust emissions suggest that dust may have played a significant role in amplifying past changes in the African hydroclimate and that inclusion of accurate dust fields may help resolve the consistent underestimation of past African monsoon variations by climate models (*20*). However, efforts to estimate the magnitude of past dust-related climate and biogeochemical impacts [for example, the studies of Pausata *et al.* (*21*), Eugster *et al.* (*22*), and Murphy *et al.* (*23*)] have been limited by the lack of quantitative reconstructions of long-range dust transport. Existing dust flux records primarily come from within 150 km of the African coast, at sites where eolian inputs are dominantly coarse (>10 μm) (*15*, *24*, *25*) and likely represent proximal dust sources. Estimates of long-range transport have proven difficult to obtain because of low sedimentation rates in open-ocean sites and mixing with fluvial sediments in quickly accumulating sites along western Atlantic continental margins (*26*).

Here, we provide quantitative constraints on changes in the trans-Atlantic transport of African dust over the last 23 ky. Our primary

[1]Department of Earth, Atmospheric and Planetary Sciences, Massachusetts Institute of Technology, Cambridge, MA 02139, USA. [2]Woods Hole Oceanographic Institution, Woods Hole, MA 02543, USA. [3]Department of Civil and Environmental Engineering, Massachusetts Institute of Technology, Cambridge, MA 02139, USA. [4]Department of Geology and Geophysics, Yale University, New Haven, CT 06511, USA. [5]Department of Earth and Environment, Boston University, Boston, MA 02215, USA. [6]Department of Earth and Environmental Sciences, Columbia University, New York, NY 10027, USA. [7]Lamont-Doherty Earth Observatory, Columbia University, Palisades, NY 10964, USA.
*Present address: Center for Research and Exploration in Space Science and Technology and NASA/Goddard Space Flight Center, Greenbelt, MD 20771, USA; Department of Astronomy, University of Maryland, College Park, MD 20742, USA.
†Corresponding author. Email: davidmcg@mit.edu

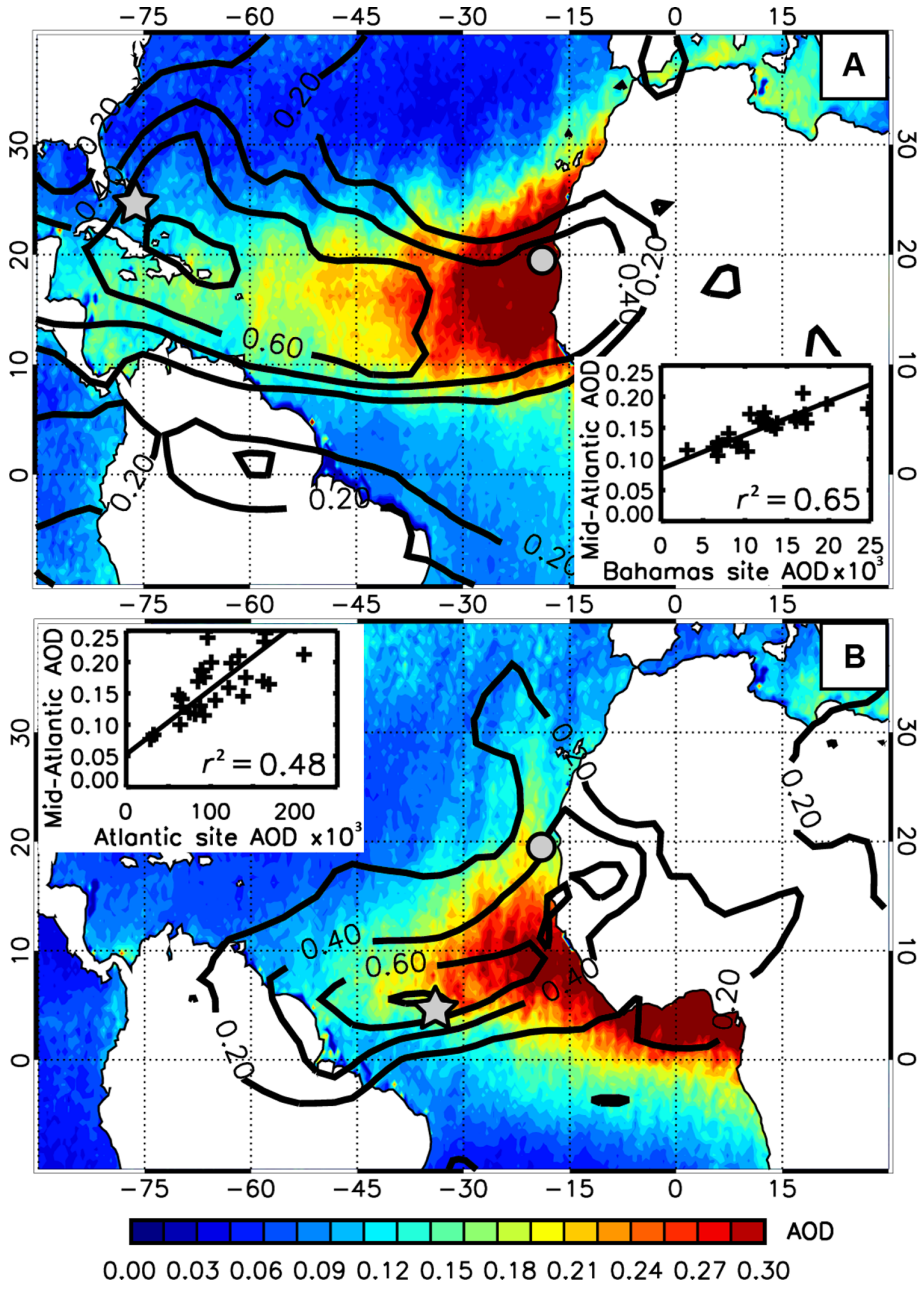

Fig. 1. Modern dust transport over the North Atlantic basin. (**A**) Map of boreal summer [June-July-August-September (JJAS)] dust aerosol optical depth (AOD) (color bar) over the North Atlantic showing the transport of African dust across the basin. Contours show r^2 values for the relationship between dust deposition at the Bahamas core sites (100GGC and 103GGC, indicated by the star) and dust loading over the rest of the North Atlantic in the Goddard Earth Observing System–Chemistry (GEOS-Chem) model (*3*). Correlations are significant for $r^2 > 0.2$. Inset shows correlation between modeled mean dust AOD over the Bahamas and dust AOD averaged over the mid-Atlantic (0°N to 30°N and 0°W to 50°W) in JJAS for each year from 1982 to 2008. (**B**) As in (A), but for boreal winter [December-January-February-March (DJFM)] and with spatial correlations calculated for the central TNA core site (VM20-234, indicated by the star). The circle shows the site of the African margin flux record shown in Fig. 2 (OCE437-7 GC68). Dust AOD data are from the 558-nm nonspherical AOD retrieval averaged over May to September between 2004 and 2008 from the Multiangle Imaging Spectroradiometer (MISR) (*76*).

reconstruction is based on terrigenous sediment fluxes in two cores from the Northwest Providence Channel near the Bahamas (Fig. 1 and fig. S1) (OCE205-2 100GGC: 26.0612°N, 78.0277°W, 1057-m water depth; OCE205-2 103GGC: 26.0703°N, 78.05617°W, 965-m water depth). This region receives African dust during the summer (*27*), and geochemical data indicate that African dust is the dominant (>80%) supplier of noncarbonate material to Bahamas sediments (*11*). Channel sediments accumulate quickly during interglacial periods (~10 cm/ky) due to high rates of aragonite production on the Bahama Banks, followed by resuspension and pelagic deposition of this carbonate (*28*). This rate is higher by factors of 4 to 10 than typical open-ocean sedimentation rates, offering a Holocene record minimally affected by bioturbation. During the last glacial period and deglaciation, sedimentation rates average 2 cm/ky because of reduced

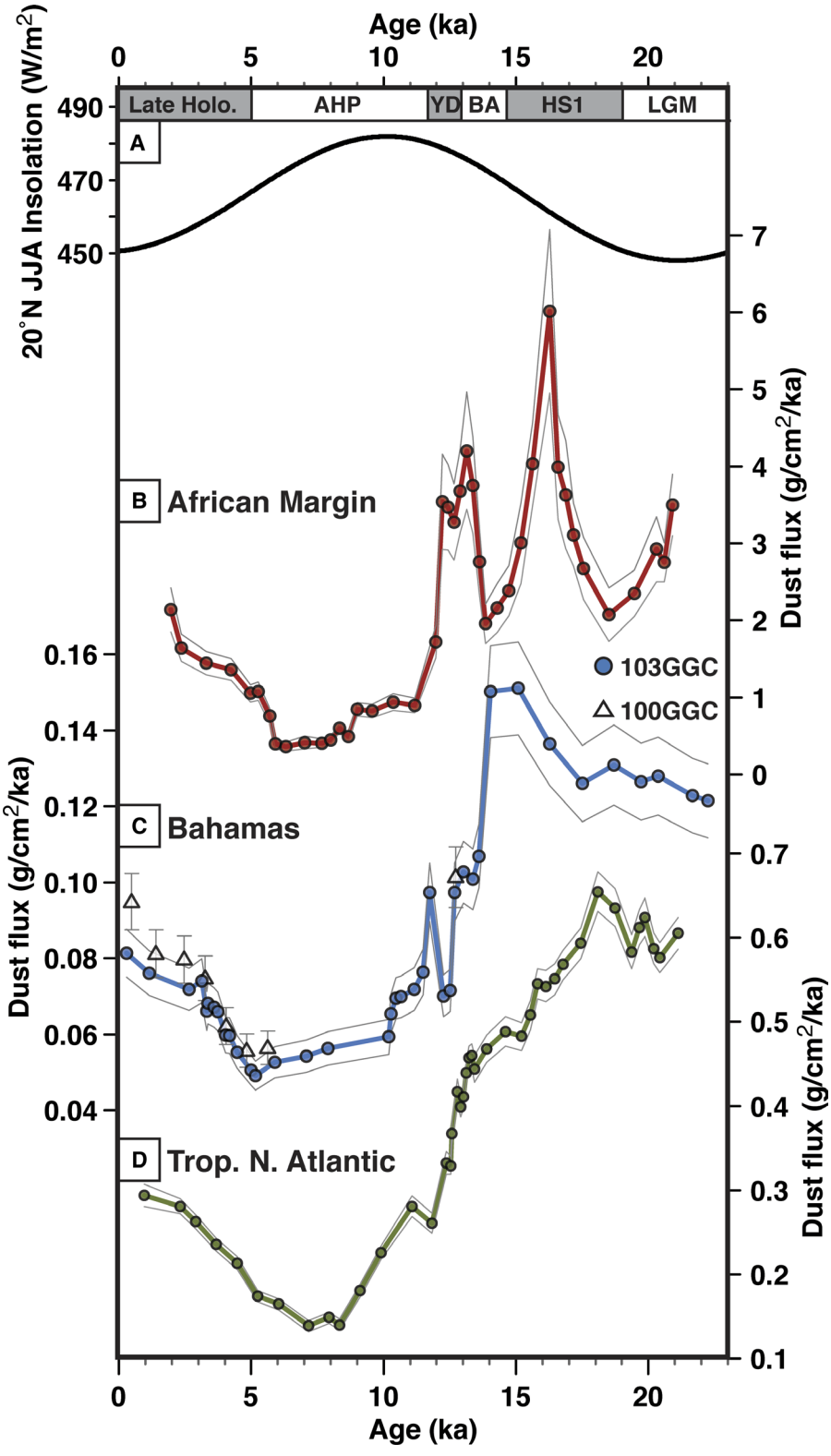

Fig. 2. African dust fluxes over the last 23 ky from locations spanning the low-latitude North Atlantic. (**A**) Summertime [June-July-August (JJA)] insolation at 20°N (*77*). (**B**) Dust flux reconstruction at northwest African margin site OCE437-7 GC68 (*15*). (**C**) Dust flux reconstructions from Bahamas sediment cores 100GGC (white triangles) and 103GGC (blue circles). (**D**) Dust flux reconstruction from TNA core VM20-234. The portion of the Bahamas record before 13 ka and the entirety of the VM20-234 record are not expected to record the amplitude or timing of millennial-scale changes in dust deposition due to low sedimentation rates. 1σ uncertainties are shown for each record's dust fluxes. Time intervals indicated at the top of the plot are as follows: AHP, African Humid Period; YD, Younger Dryas stadial; BA, Bølling-Allerød interstadial; HS1, Heinrich Stadial 1; LGM, Last Glacial Maximum.

local carbonate production, producing records that are substantially smoothed by bioturbation (*28*).

To test whether similar changes occurred in the winter dust plume, we present a terrigenous flux record from the central TNA (VM20-234: 5.33°N, 33.03°W, 3133-m water depth), where African dust deposition during winter and spring (*1*) is the primary source of terrigenous inputs (Fig. 1B) (*29*). Sedimentation rates at this site (~3 cm/ky) are high enough to resolve orbital and glacial-interglacial changes, but bioturbation is expected to obscure millennial-scale changes and may reduce the amplitude of precessional-scale changes.

We explore the potential climate impacts of these reconstructed changes in the North African dust plume using idealized simulations of the radiative impact of reduced dust loading over the TNA. Recent modeling studies have primarily focused on the impact of dust loading over the African continent. These studies demonstrate strong sensitivity to both dust optical properties and surface albedo (*21*, *30*–*32*) and generally do not include potentially significant indirect effects of dust on cloud properties and precipitation (*5*, *6*, *33*). Observational evidence suggests that dust loading over the TNA may also have significant impacts because North African dust emissions appear to be part of coupled system involving amplifying feedbacks between trade wind strength, dust radiative forcing, low-level cloud cover, and TNA SSTs that may be a primary driver of multidecadal climate variability in the low-latitude Atlantic (*5*, *9*, *33*). The strong correlations between dust fluxes and proxy records of trade wind strength along the northwest African margin during the deglaciation and Holocene (*14*, *34*) suggest that this coupled variability may have been a key feature of past regional climate changes, but the poor representation of this coupling in general circulation models (GCMs) presently limits the investigation of its importance (*30*, *33*).

In an effort to offer first-order insights into the potential impacts of the changes in long-range Saharan dust transport reconstructed here, we simulate the impact of reduced dust loading over the TNA, as observed in the mid-Holocene. These simulations test whether dust-related changes in TNA SSTs may have amplified precessional forcing of the Atlantic Intertropical Convergence Zone (ITCZ) and West African monsoon during the AHP, affected wind speeds over dust source regions, and helped accelerate mid-Holocene drying of North Africa.

RESULTS

Evaluation of Bahamas and central TNA core sites as archives of African dust emissions

Measurements of airborne dust concentrations in south Florida, just west of the Bahamas, show a clear peak in summer, consistent with supply from the summer African dust plume (*27*, *35*, *36*). Geochemical and mineralogical data indicate that African dust is the dominant supplier of noncarbonate material to Bahamas soils and nearby ocean sediments (*11*, *37*). Some contribution of windblown dust from North America is possible during glacial periods, when substantial dust sources existed in the interior United States (*38*). However, even in Bahamas soils integrating glacial-interglacial cycles, North American contributions are estimated as <20% of total noncarbonate material, with the remaining >80% coming from African dust (*11*). North American dust sources were inactive in most of the Holocene (*38*) and are thus particularly unlikely to affect the Holocene records in the Bahamas cores.

To test whether the terrigenous component of our samples is consistent with African dust, we measured the abundance of Zr, Sc, and Th, elements associated with the terrigenous fraction and resistant to diagenetic alteration (see Materials and Methods). The data agree well with previously published data from Bahamas soils and show clear similarity with the composition of African dust collected in Barbados (fig. S7) (*11*). The composition of Caribbean volcanics has only limited overlap with the African dust and Bahamas fields, suggesting negligible contributions from volcanic sources to Bahamas sediments. Zr-Sc-Th data from Mississippi Valley Loess also overlap with African dust and Bahamas sediments (*11*), and North American sources cannot be excluded based on these trace elements. However, as discussed above, previous studies suggest that North American dust sources do not contribute substantially to Bahamas sediments, particularly during the Holocene.

In the central TNA near core site VM20-234, African dust has been demonstrated to be the dominant supplier of trace metals (Al, Fe, and Th) to the surface ocean (*39*, *40*). Radiogenic isotope measurements ($^{87}Sr/^{86}Sr$ and $^{143}Nd/^{144}Nd$) in nearby sediments also support African dust as the primary source of lithogenic material at 5°N in the central TNA (*29*). The distance of this core site from continental margins and its location on a local bathymetric high minimizes the potential for fluvial or downslope inputs of lithogenic material. Mid-ocean ridge volcanics have very low ^{232}Th concentrations [average concentration of 0.22 μg/g (*41*), compared to 13.7 μg/g in fine-grained African dust (*11*)] and thus are unlikely to influence ^{232}Th accumulation rates, the basis for our dust flux reconstructions.

Modern-day dust deposition measurements offer a test of the accuracy of our reconstructed dust fluxes. Estimates of Saharan dust deposition fluxes in south Florida from the 1980s to the 1990s range from 0.11 to 0.15 g/cm^2 per ka (*36*, *42*, *43*), similar to our Bahamas core-top estimates of 0.08 to 0.09 g/cm^2 per ka. Because core-top data average several centuries, whereas the Florida estimates represent only a few years, the difference could reflect a recent enhancement in African dust deposition or short-term variability captured by the Florida estimates. Alternatively, lower dust fluxes in the Bahamas could result from higher mean summer precipitation in south Florida—and thus greater wet deposition of airborne dust—or a small systematic offset in ^{230}Th supply to the core sites (see the Supplementary Materials).

In the central TNA, dissolved aluminum concentrations measured in surface waters along the A16N transect between 3°N and 10°N at ~25°W indicate modern dust deposition rates of 0.2 to 0.3 g/cm^2 per ka (*39*), very similar to core-top dust flux estimates of 0.28 g/cm^2 per ka at VM20-234. This similarity suggests that hydrothermal activity near this site does not substantially bias dust flux estimates at VM20-234 (see the Supplementary Materials).

We test whether dust loading over these sites is representative of the broader North African dust plume using the GEOS-Chem model. These simulations include prognostic dust emissions driven by MERRA (Modern-Era Retrospective Analysis for Research and Analysis) reanalysis meteorology from 1982 to 2008, and they capture the observed seasonality, transport, and temporal trends of African dust (*3*). We find a strong correlation between dust AOD over the Bahamas and summer dust AOD over the TNA ($r^2 = 0.65$, $P < 0.001$) (Fig. 1A). A similarly strong correlation exists between dust AOD over the central TNA site and winter dust AOD over the TNA ($r^2 = 0.48$, $P < 0.001$) (Fig. 1B). These findings suggest that the Bahamas and central TNA sites are well suited to reconstruct the African dust plume in summer and winter, respectively.

Dust flux reconstructions from the Bahamas and central TNA sediments

Dust fluxes were reconstructed in two sites from the Northwest Providence channel near the Bahamas and in one site in the central TNA. Accumulation rates were determined by $^{230}Th_{xs}$ normalization, which provides accumulation rate estimates that are minimally affected by lateral supply (see Materials and Methods) (*44*). The terrigenous fraction was determined from ^{232}Th concentrations using measurements of the ^{232}Th content of African dust collected in Barbados (*11*, *45*). Dust fluxes in the two Bahamas cores agree with each other within uncertainty (Fig. 2). As described above, core-top dust fluxes in both the Bahamas and tropical Atlantic sites are similar to modern dust fluxes measured near the sites, supporting the fidelity of the reconstructed dust fluxes.

Over the last 12 ky, Bahamas dust fluxes closely parallel African margin records at millennial-scale resolution (Fig. 2). On both sides of the Atlantic, dust fluxes fall quickly at the end of the YD (~12 ka) and decline throughout the AHP with minimum fluxes at around 6 ka, approximately 40% lower than core-top values. Dust fluxes rise rapidly around 5 ka and then rise gradually toward the core top. The steady rise in dust fluxes over the last 4 ky agrees with African margin dust flux records (Fig. 2B) (*14*, *15*) but does not agree with a record of terrigenous accumulation in a south Florida peat bog taken to represent Saharan dust inputs, which shows a rapid decline in terrigenous fluxes after 2.8 ka (*13*).

The difference between minimum AHP fluxes and recent dust fluxes is smaller in the Bahamas (~40% lower at 6 ka) than on the African margin (~75 to 80% lower). This difference most likely relates to the fact that the African margin sites reflect proximal dust sources, whereas the Bahamas record presumably samples a large region of northwest Africa. In addition, the difference may reflect the seasonality of dust transport (summer in the Bahamas, winter along the northwest African margin) or more efficient transport to sites such as the Bahamas at the north edge of the modern dust plume in association with a northward displacement of the ITCZ at 6 ka.

It is difficult to test whether the end-AHP rise in dust flux occurred with the same timing and abruptness in the Bahamas as on the African margin because the transport time of sediments from bank tops to channel sediments is approximately 400 to 600 years (*46*), imparting a lag and smoothing the record in the Bahamas cores. Despite this uncertainty, the Bahamas record suggests strong similarity to the changes recorded on the African margin throughout the Holocene.

Before 13 ka, the Bahamas record is substantially affected by bioturbation due to low sedimentation rates. Dust fluxes are a factor of ~1.5 greater than core-top values during the Last Glacial Maximum (LGM; 19 to 23 ka), similar to records from the African margin. Dust fluxes then rise to maximum levels during the deglaciation (~12 to 19 ka). African margin records resolve peak dust fluxes during HS1 and the YD, whereas the Bahamas record shows a single peak centered at 14 to 15 ka (Fig. 2).

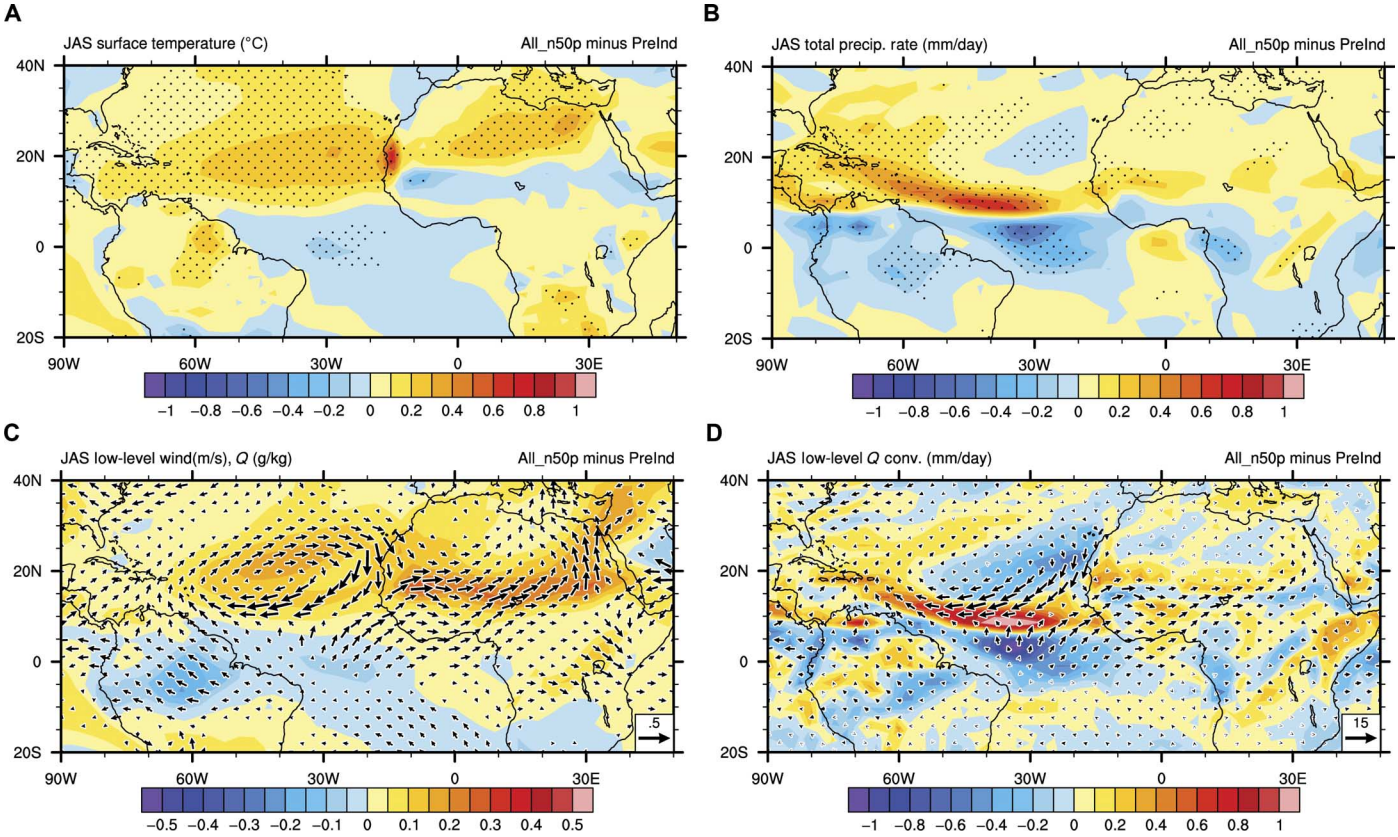

Fig. 3. Coupled climate model simulation of the impacts of reduced dust loading over the TNA. (**A** to **D**) JAS changes in the reduced dust simulation ("All_n50p") relative to the preindustrial control for (A) surface temperature (°C), (B) precipitation (mm/day), (C) low-level specific humidity (g/kg) and winds (vectors; m/s), and (D) low-level water vapor convergence (mm/day) and water vapor transport (vectors; kg·m/s). Low level is defined as an average from the surface to approximately 830 hPa. Stippling in (A) and (B) indicates significance at $P < 0.1$.

To simulate the impacts of bioturbation on the deglacial record from the Bahamas, we use a simple bioturbation model that assumes complete mixing of a surface layer (*47*, *48*). The model incorporates measured sedimentation rates from Bahamas core 103GGC and a bioturbation depth of 8 cm based on ^{210}Pb profiles measured in Bahamas slope sediments (*47*). As an input function, we used the dust deposition record from African margin core GC68 (Fig. 2B) to test whether the deglacial record from the Bahamas is consistent with a dust input history that tracks the African margin record.

After the African margin record was passed through the model, it showed a single peak at 13 to 14 ka, similar to the observed Bahamas record (fig. S4). The 1-ka difference between the observed peak in Bahamas dust deposition (14 to 15 ka) and the peak estimated by the bioturbation model (13 to 14 ka) may reflect age model errors in the Bahamas sediments near the transition from low to high sedimentation rates because changes in sediment composition can cause foraminiferal tests to be up to 1.5 ka older than the coexisting bulk sediment near this transition (*47*).

The similarity between the bioturbated African margin record and the observed Bahamas record during the deglaciation suggests that the Bahamas also experienced peak dust fluxes during HS1 and the YD. This conclusion implies that mixing causes the Bahamas record to underestimate the magnitude of the peak deglacial dust fluxes. On the basis of the difference in peak fluxes between the smoothed (fig. S4) and unsmoothed (Fig. 2B) African margin record (3.5 g/cm^2 per ka after smoothing versus 6 g/cm^2 per ka observed in HS1), peak dust fluxes in the Bahamas during HS1 may have been approximately a factor of 2 larger than the peak value of 0.16 g/cm^2 per ka or a factor of 4 higher than core-top fluxes.

The central TNA core shows minimum dust fluxes during the AHP that are ~50% of core-top fluxes. The greater smoothing by bioturbation in this core makes this a minimum estimate of the reduction in the winter dust plume during the AHP. Together with the Bahamas results, these results indicate that the AHP Saharan dust plume was reduced in both winter and summer by approximately 50%. In the central TNA, the deglaciation and LGM are marked by larger increases in dust flux than in the Bahamas [approximately a factor of 2.5, similar to previous results from the Sierra Leone rise (*49*)], perhaps due to a southward shift of the Atlantic ITCZ (*50*) and thus more efficient transport to the site.

GCM investigation of the impact of reduced dust loading in the TNA

We conducted idealized GCM experiments focused on the impact of changing dust loads over the TNA, the parameter reflected in the records presented here. We tested the effect of reduced TNA dust loading using both a fully coupled GCM and a slab ocean configuration of the same model [National Center for Atmospheric Research (NCAR) Community Earth System Model (CESM) with Community Atmosphere Model version 4 (CAM4) atmospheric model]. We reduced dust loading by 50% over the TNA (5°N to 30°N and 80°W to 15°W) in all seasons under preindustrial boundary conditions and compared to control simulations. Dust loads over the North African continent were kept the same in all simulations. The fully coupled simulations were run for 200 years, and the results were averaged over the last 180 years. The slab ocean simulations were run for 300 years, and the results were averaged over the last 280 years. The results are intended to isolate the impact of changing dust loads over the TNA, complementing and extending previous work focused on changes in dust loading over the continent (*31*) and their interaction with mid-Holocene vegetation and insolation (*21*). Here, we describe the results from coupled simulations and then compare them with the results from the slab ocean model.

The impact of windblown dust on modern and past North African climate is an area of active investigation, with substantial uncertainties related to dust's optical parameters (*51*), the ability of GCMs to simulate dust emissions and transport (*52*), and the indirect effects of dust on cloud properties (*53*). The default dust optical parameters in CAM4 are likely to overestimate dust's direct effects on incident shortwave radiation at the surface, and they do not include its longwave impacts (*51*). Longwave radiation changes are a small fraction of dust-driven radiative perturbations over the ocean, and they have been argued to be negligible in past studies of dust-related SST impacts in the TNA (*4*). Moreover, dust-related reductions in mid-tropospheric water vapor cause roughly equal and opposite longwave forcing at the surface, cancelling longwave effects of dust loading (*4*).

The total clear-sky radiative perturbation at the surface in our 50% reduction simulations is +4.94 W/m^2 averaged over the TNA (+4.95 W/m^2 for the slab ocean simulations) compared to the control simulation. This radiative perturbation is ~67% of the estimated clear-sky surface direct radiative impact for the modern dust plume (−7.4 ± 1.5 W/m^2) (*3*), consistent with the understanding that CAM4 overestimates dust's direct effects. Given the fact that indirect radiative impacts of dust are likely to be similar in magnitude and of the same sign (*5*) and are not included in these or most other simulations, we consider this magnitude to be a reasonable first-order estimate of the impacts of the reduced dust loads indicated by our reconstructions during the AHP and useful for estimating the sensitivity of regional climate to dust-related changes in SSTs.

TNA SSTs warm significantly in summer [July-August-September (JAS)] in response to reduced dust loading, with maximum anomalies of 0.3°C near the West African margin and an average warming across the TNA (5°N to 30°N and 15°W to 80°W) of 0.15°C (Fig. 3A). The maximum SST anomalies in this simulation are similar to an estimate of 0.3° to 0.4°C SST warming in the TNA in response to a sustained 40 to 60% reduction in dust loading derived by Evan *et al.* (*4*) using observational estimates of dust optical properties and an ocean mixed layer model. The dust-driven warming produces anomalous meridional SST and sea-level pressure gradients in the tropical Atlantic (Fig. 3A and fig. S8). The low-level specific humidity anomalies associated with TNA warming lead to a northward displacement of the Atlantic ITCZ (Fig. 3, B and C), with the JAS precipitation centroid (the center of mass of tropical precipitation) between 10°W and 60°W shifting north by 0.23°. In the slab ocean experiment, the increase of summer TNA SSTs averages 0.18°C. The northward shift of ITCZ over the ocean is similar to that in the coupled experiment, producing a shift of 0.31° between 10°W and 60°W (fig. S9). These ITCZ changes are substantial given the sensitivity of atmospheric heat transport to ITCZ position (*54*) and the small magnitude of zonal mean changes in precipitation centroid position estimated for past climates (*55*).

Increased TNA SSTs in the coupled reduced dust experiment also significantly increase precipitation over northwest Africa (Fig. 3B), with JAS anomalies reaching 0.2 to 0.3 mm/day in the western Sahel and 0.1 mm/day in the western Sahara. These changes are substantial compared to JAS precipitation rates of ~2.6 mm/day in the Sahel and ~0.25 mm/day in the western Sahara in the control simulation (fig. S10). Altered sea-level pressure gradients (fig. S8) drive southwesterly

wind anomalies that increase moisture transport convergence over the continent (Fig. 3, C and D), allowing northward penetration of monsoon rains into the Sahel and western Sahara. In the slab ocean experiment, the southwesterly wind anomalies are weaker but still lead to substantial increases in precipitation, reaching 0.5 mm/day in the western Sahel and southwestern Sahara (fig. S9). Overall, precipitation changes in the coupled and slab ocean simulations look qualitatively similar, reflecting both local and more remote responses to the warming over the TNA region where the dust forcing was applied. In both experiments, the spatial structure of the precipitation response to dust reduction looks similar to a correlation map between local precipitation and summer TNA surface temperature in the unperturbed slab ocean simulation (fig. S11). This similarity suggests that the observed precipitation responses in the reduced dust experiments are primarily due to the TNA SST warming in response to reduced dust loading.

The reduced dust simulation also shows a strong warming and reduced surface pressures in the central Sahara (Fig. 3A and fig. S8). This warming results from increased water vapor over the Sahara, which drives surface heating through increased trapping of outgoing longwave radiation. The resulting reduction in surface pressure strengthens the Saharan heat low, leading to cyclonic wind anomalies (Fig. 3C) that insulate the region from mixing with cooler midlatitude air, augmenting the warming. The surface wind response weakens climatological northerly and northeasterly winds in the Sahara (fig. S10), potentially decreasing dust emissions in a manner similar to modern Saharan heat low variability (*56*).

DISCUSSION

The Bahamas and tropical Atlantic dust flux records presented here provide quantitative constraints on variations in long-range African dust transport over the last 23 ky. Trans-Atlantic dust transport appears to have been approximately 40 to 50% lower than at present during the early and mid-Holocene and 50 to 150% higher than at present during the LGM and deglaciation. Similar changes are recorded at sites underlying both the summer and winter dust transport paths. Although our records cannot resolve millennial-scale variability during the deglaciation, bioturbation modeling suggests that peak dust loading is most likely during HS1 and the YD, consistent with African margin records, with maximum dust fluxes reaching as much as a factor of 4 higher than core-top values in the Bahamas. These results provide a much improved basis for estimating dust-related radiative forcing in past climates.

In addition, the data provide a new basis for testing hypotheses linking dust deposition to nitrogen fixation in the North Atlantic (*10*), carbonate production in the Bahamas (*57*), coral reef health in the Caribbean (*58*), and terrestrial ecosystem productivity in the western Atlantic (*12*); future work should examine the response of each of these systems to the reconstructed changes in dust delivery. Because nitrogen isotope records from the TNA do not show evidence for a mid-Holocene reduction in nitrogen fixation (*59*, *60*), our results suggest that a factor of 2 reduction in dust-related iron delivery to the TNA relative to the present is not sufficient to limit nitrogen fixation. This result lends support to the results of biogeochemical model simulations (*61*) and to the hypothesis that TNA nitrogen fixation is limited by excess phosphate availability rather than iron (*62*).

Building on the constraints our results place on changes in long-range Saharan dust transport, this study explores the sensitivity of regional climate to dust-driven SST changes. Previous studies have identified insolation-driven SST (*63*) and vegetation (*64*) changes as important amplifying feedbacks on Late Quaternary North African climate changes; however, simulations of 6-ka climate that include these feedbacks still fail to reproduce the northward expansion of monsoon precipitation indicated by pollen data (*20*). Recent work has begun to explore the role of dust in 6-ka climate, focusing on the direct radiative impact of dust over the African continent (*21*). This impact is highly dependent on surface albedo. Over low-albedo land surfaces, the reduction in surface radiation due to dust dominates, leading to reduced precipitation with increased dust (*32*). Over high-albedo surfaces, this impact is less important and competes with a "heat pump" effect, in which absorption of radiation by dust heats the atmosphere and increases convection, with the net impact on precipitation being highly sensitive to differences in dust grain size, optical properties, and altitude (*21*, *30*–*32*). As a result, a reduction in dust amplifies monsoon expansion in a simulation with a densely vegetated (surface albedo of 0.15) Sahara (*21*), but simulations with modern vegetation distributions differ as to the sign and magnitude of dust's impact on North African precipitation (*21*, *30*–*32*).

Our GCM experiments focus on the complementary question of the impact of dust loading over the TNA using a simplified radiative perturbation similar in magnitude and spatial scale to dust's direct radiative effects. Because of the low albedo of the sea surface, dust's direct impacts are dominated by its effect on incident shortwave radiation (*4*). Our results suggest that small changes in TNA SSTs due to reduced long-range African dust transport (+0.15°C) may significantly amplify changes in Atlantic ITCZ position and West African precipitation independent of dust's uncertain effects over the continent. Surface winds in Saharan dust source regions also weaken in response to SST warming in our simulation, potentially leading to further reduction in dust emissions. Our results point to coupled dust–SST–Saharan heat low changes that may play a role in both Holocene and recent decadal climate changes in the region (*33*, *56*). The dust-SST link explored here may also play a role in the weakening of the monsoon and southward shift of the Atlantic ITCZ accompanying maximum dust emissions during Heinrich events (*23*). The finding of significant dust-SST-climate links is consistent with studies of recent climate variability using observations and simple models (*4*, *9*, *33*) but at odds with some previous GCM studies using different optical parameters for dust (*21*, *30*).

Our work demonstrates the importance of constraining dust's effects on regional SSTs in both past and modern climates. Dust optical properties are not well known, and radiative impacts are sensitive to the details of the size and optics chosen (*32*, *65*). Updates to dust optical parameters in CAM4 reduce dust's direct radiative impact at the surface by approximately a factor of 3 (*51*), diminishing simulated SST responses relative to the results shown here. Potentially offsetting this change, indirect effects of dust not included in this or most other modeling studies may cause substantial reductions in surface radiation over the TNA. Observational evidence suggests increases in low-level cloud cover over the TNA in response to dust loading, due to both increased atmospheric column stability (*5*) and decreased cloud droplet size (*6*, *66*, *67*), causing a net reduction in surface radiation. Dust's indirect effects may also affect precipitation patterns through changes in cloud optical properties, droplet size, and convective intensity. These impacts are sensitive to factors such as dust hygroscopicity, size, altitude, and optical properties (*68*–*70*), but observational data from the region suggest

that the presence of dust in clouds generally suppresses precipitation by reducing droplet size (*67*, *70*).

Future work will be required to examine how dust-related increases in SSTs interact with mid-Holocene insolation and vegetation changes. As one example of such an interaction, insolation-related decreases in cloud cover over the TNA would increase the impact of changes in dust loading on SSTs. Of particular importance will be simulations with prognostic dust emissions, allowing inclusion of dust's emission, transport, deposition, and radiative impacts in a self-consistent framework (*23*, *71*, *72*). These simulations have the potential to capture feedbacks of SSTs on dust emissions suggested by our results but will require additional work to improve representations of North African source areas (*52*, *73*) and depositional processes (*36*). Models that simulate the transient evolution of dust, lakes, vegetation, and regional climate through the beginning and end of the AHP may also provide insights into the role of land surface and aerosol feedbacks in monsoon transitions. Our records of long-range transport of fine-grained dust may contribute to these simulations by offering better constraints on dust loading in the middle and upper troposphere above North Africa than more proximal records containing mainly coarse-grained (>10 μm) dust.

This analysis, in combination with recent studies (*21*, *23*, *30*), suggests that inclusion of accurate dust loading in simulations of past climate—rather than the preindustrial dust fields currently used—may significantly improve models' representation of monsoon changes in North Africa and shifts of the Atlantic ITCZ. More fundamentally, the records presented here demonstrate coherent, high-amplitude fluctuations in the North African dust plume on both sides of the Atlantic and in both winter and summer in response to past climate changes, offering quantitative targets for future investigations of dust's impacts on regional climate and biogeochemistry.

MATERIALS AND METHODS

Dust flux measurements

Sediment fluxes were calculated using the $^{230}Th_{xs}$ normalization method (*44*). ^{230}Th has a known and constant production rate in the water column from ^{234}U. Because Th has a short (decades) residence time in the water column, Th is adsorbed to falling particles and deposited in sediments at a rate that is fast relative to the time scale of advection of dissolved Th. Sedimentary concentrations of adsorbed ^{230}Th ($^{230}Th_{xs}$) may thus be taken to be inversely proportional to the vertical rain rate of sediments. The ^{230}Th-normalized sediment flux F for each sample is calculated in units of g/cm^2 per ka as

$$F = \frac{\beta z}{(^{230}Th_{xs})} \quad (1)$$

where β is the ^{230}Th production rate in seawater (0.0263 dpm/m^3 per year), z is the water depth in meters, and ($^{230}Th_{xs}$) is the measured ^{230}Th activity after corrections for ^{230}Th supported by ^{238}U in detrital sediments, ^{230}Th supported by authigenic ^{238}U precipitated from seawater, and radioactive decay of unsupported ^{230}Th since deposition. In most sediments, authigenic U is precipitated because of reducing conditions, but in the Bahamas sediments, it is dominantly hosted by aragonite precipitated on the bank tops. Estimates of detrital ^{230}Th and authigenic U assume a detrital $^{238}U/^{232}Th$ activity ratio of 0.6 ± 0.1, but our results are not sensitive to this ratio. Water depths in the Bahamas were corrected for deglacial sea-level change. Methods for U and Th isotope measurements are described in the Supplementary Materials.

Dust fluxes were calculated from measurements of ^{230}Th-normalized fluxes of ^{232}Th. Mean ^{232}Th concentrations are 13.7 ± 1.0 μg/g in the <5-μm fraction of African dust sampled in Barbados (*11*). The short residence time of Th in shallow waters suggests that most ^{232}Th dissolved from dust should be quickly scavenged and deposited locally. Dust fluxes (F_{dust}) in units of g/cm^2 per ka were calculated as

$$F_{dust} = \frac{F \cdot [^{232}Th]}{13.7} \quad (2)$$

where [^{232}Th] is the measured concentration of ^{232}Th in μg/g, and 13.7 is the concentration of ^{232}Th in African dust, also in μg/g. All U-Th data are included in data file S1.

Trace element analyses

Samples weighing 30 mg were dissolved in the same manner as for U-Th analyses but without addition of spike solutions. A procedural blank and two aliquots of the NIST-1C carbonate standard were also dissolved. Samples were then diluted and measured using a VG Plasma Quad ExCell quadrupole inductively coupled plasma mass spectrometry at Boston University. Calcium was added in solution to several U.S. Geological Survey standards to achieve similar Ca concentrations to samples, and the standards were run to develop calibration curves for a suite of trace and minor elements. A Ca-spiked aliquot of dissolved BHVO-2 standard was run as an unknown to check accuracy, with results for Zr, Sc, and Th all within 5% of accepted values. Two sets of replicates were prepared among the sample set, with an average reproducibility better than 6% for Zr, Sc, and Th. All Zr, Sc, and Th data are included in data file S3.

GCM experiments

Here, we use the coupled GCM developed by the NCAR CESM (version 1.0.4). The horizontal resolution is 1.9° × 2.5° for the atmospheric component, and gx1v6 (roughly 1° globally and further refined near the equator) for the oceanic component. The atmospheric component CAM4 uses prescribed bulk aerosols, and only the direct and semidirect (that is, effects of absorbing aerosols on cloud properties and thus radiation by warming the air) radiative effects of aerosols are considered. More details about the model can be found in studies by Neale *et al.* (*74*) and Gent *et al.* (*75*). We conducted two simulations using preindustrial boundary conditions. The first simulation is a control and the other is a perturbed experiment in which dust concentrations are reduced by 50% over the TNA (5°N to 30°N and 80°W to 15°W) in all size bins and during all seasons. Both simulations were run for 200 years, and the means for the last 180 years were analyzed.

To isolate the role of the ocean mixed layer response to the dust forcing, we conducted two similar simulations (preindustrial and reduced dust) but using a slab ocean model configuration with a slightly different version (1.0.5) of CESM. In these slab ocean simulations, a spatially varying mixed layer depth is specified, and a spatially and monthly varying heat flux (that is, the so-called Q-flux) is used to account for the processes that are not explicitly simulated, such as advection and mixing. Knowing this information, mixed

layer temperature is then interactively calculated on the basis of surface energy fluxes. Both simulations were run for 300 years, and the means for the last 280 years were analyzed.

SUPPLEMENTARY MATERIALS

Supplementary material for this article is available at http://advances.sciencemag.org/cgi/content/full/2/11/e1600445/DC1

Supplementary Materials and Methods

fig. S1. Map showing core sites for Bahamas cores OCE205-2 100GGC and 103GGC.

fig. S2. Age-depth plots for OCE205-2 100GGC and 103GGC.

fig. S3. Comparison of focusing factors and reconstructed dust fluxes in core 103GGC.

fig. S4. Test of the impact of bioturbation on the deglacial portion of the Bahamas record.

fig. S5. Map showing core site for core VM20-234 along the Mid-Atlantic Ridge.

fig. S6. Age-depth plot and sedimentation rates for VM20-234.

fig. S7. Ternary diagram comparing the trace element compositions of Bahamas sediments and soils and potential sources of terrigenous sediment.

fig. S8. Sea-level pressure changes in the GCM experiment.

fig. S9. Slab ocean simulation of the impacts of reduced dust loading over the subtropical North Atlantic.

fig. S10. Climate mean state from the preindustrial control run of the coupled climate model.

fig. S11. Relationship between surface temperatures and rainfall in the preindustrial slab ocean control simulation.

data file S1. U-Th data and dust fluxes.

data file S2. Radiocarbon data from core VM20-234.

data file S3. Trace element data from Bahamas sediments.

References (*78*–*94*)

REFERENCES AND NOTES

1. D. A. Ridley, C. L. Heald, B. Ford, North African dust export and deposition: A satellite and model perspective. *J. Geophys. Res. Atmos.* **117**, D02202 (2012).
2. G. Gläser, H. Wernli, A. Kerkweg, F. Teubler, The transatlantic dust transport from North Africa to the Americas—Its characteristics and source regions. *J. Geophys. Res. Atmos.* **120**, 11231–11252 (2015).
3. D. A. Ridley, C. L. Heald, J. M. Prospero, What controls the recent changes in African mineral dust aerosol across the Atlantic? *Atmos. Chem. Phys.* **14**, 5735–5747 (2014).
4. A. T. Evan, D. J. Vimont, A. K. Heidinger, J. P. Kossin, R. Bennartz, The role of aerosols in the evolution of tropical North Atlantic Ocean temperature anomalies. *Science* **324**, 778–781 (2009).
5. O. M. Doherty, A. T. Evan, Identification of a new dust-stratocumulus indirect effect over the tropical North Atlantic. *Geophys. Res. Lett.* **41**, 6935–6942 (2014).
6. Y. J. Kaufman, I. Koren, L. A. Remer, D. Rosenfeld, Y. Rudich, The effect of smoke, dust, and pollution aerosol on shallow cloud development over the Atlantic Ocean. *Proc. Natl. Acad. Sci. U.S.A.* **102**, 11207–11212 (2005).
7. C. Wang, S. Dong, A. T. Evan, G. R. Foltz, S.-K. Lee, Multidecadal covariability of North Atlantic sea surface temperature, African dust, Sahel rainfall, and Atlantic hurricanes. *J. Clim.* **25**, 5404–5415 (2012).
8. J. M. Prospero, P. J. Lamb, African droughts and dust transport to the Caribbean: Climate change implications. *Science* **302**, 1024–1027 (2003).
9. A. T. Evan, G. R. Foltz, D. Zhang, D. J. Vimont, Influence of African dust on ocean–atmosphere variability in the tropical Atlantic. *Nat. Geosci.* **4**, 762–765 (2011).
10. C. M. Moore, M. M. Mills, E. P. Achterberg, R. J. Geider, J. LaRoche, M. I. Lucas, E. L. McDonagh, X. Pan, A. J. Poulton, M. J. A. Rijkenberg, D. J. Suggett, S. J. Ussher, E. M. S. Woodward, Large-scale distribution of Atlantic nitrogen fixation controlled by iron availability. *Nat. Geosci.* **2**, 867–871 (2009).
11. D. R. Muhs, J. R. Budahn, J. M. Prospero, S. N. Carey, Geochemical evidence for African dust inputs to soils of western Atlantic islands: Barbados, the Bahamas, and Florida. *J. Geophys. Res.* **112**, F02009 (2007).
12. H. Yu, M. Chin, T. Yuan, H. Bian, L. A. Remer, J. M. Prospero, A. Omar, D. Winker, Y. Yang, Y. Zhang, Z. Zhang, C. Zhao, The fertilizing role of African dust in the Amazon rainforest: A first multiyear assessment based on data from Cloud-Aerosol Lidar and Infrared Pathfinder Satellite Observations. *Geophys. Res. Lett.* **42**, 1984–1991 (2015).
13. P. H. Glaser, B. C. S. Hansen, J. J. Donovan, T. J. Givnish, C. A. Stricker, J. C. Volin, Holocene dynamics of the Florida Everglades with respect to climate, dustfall, and tropical storms. *Proc. Natl. Acad. Sci. U.S.A.* **110**, 17211–17216 (2013).
14. J. Adkins, P. deMenocal, G. Eshel, The "African humid period" and the record of marine upwelling from excess ^{230}Th in Ocean Drilling Program Hole 658C. *Paleoceanography* **21**, PA4203 (2006).
15. D. McGee, P. B. deMenocal, G. Winckler, J. B. W. Stuut, L. I. Bradtmiller, The magnitude, timing and abruptness of changes in North African dust deposition over the last 20,000 yr. *Earth Planet. Sci. Lett.* **371–372**, 163–176 (2013).
16. P. deMenocal, J. Ortiz, T. Guilderson, J. Adkins, M. Sarnthein, L. Baker, M. Yarusinsky, Abrupt onset and termination of the African humid period: Rapid climate responses to gradual insolation forcing. *Quat. Sci. Rev.* **19**, 347–361 (2000).
17. T. M. Shanahan, N. P. McKay, K. A. Hughen, J. T. Overpeck, B. Otto-Bliesner, C. W. Heil, J. King, C. A. Scholz, J. Peck, The time-transgressive termination of the African Humid Period. *Nat. Geosci.* **8**, 140–144 (2015).
18. F. Gasse, Hydrological changes in the African tropics since the Last Glacial Maximum. *Quat. Sci. Rev.* **19**, 189–211 (2000).
19. S. Weldeab, D. W. Lea, R. R. Schneider, N. Andersen, 155,000 Years of West African Monsoon and ocean thermal evolution. *Science* **316**, 1303–1307 (2007).
20. A. Perez-Sanz, G. Li, P. González-Sampériz, S. P. Harrison, Evaluation of modern and mid-Holocene seasonal precipitation of the Mediterranean and northern Africa in the CMIP5 simulations. *Clim. Past* **10**, 551–568 (2014).
21. F. S. R. Pausata, G. Messori, Q. Zhang, Impacts of dust reduction on the northward expansion of the African monsoon during the Green Sahara period. *Earth Planet. Sci. Lett.* **434**, 298–307 (2016).
22. O. Eugster, N. Gruber, C. Deutsch, S. L. Jaccard, M. R. Payne, The dynamics of the marine nitrogen cycle across the last deglaciation. *Paleoceanography* **28**, 116–129 (2013).
23. L. N. Murphy, A. C. Clement, S. Albani, N. M. Mahowald, P. Swart, M. M. Arienzo, Simulated changes in atmospheric dust in response to a Heinrich stadial. *Paleoceanography* **29**, 30–43 (2014).
24. J.-B. Stuut, M. Zabel, V. Ratmeyer, P. Helmke, E. Schefuß, G. Lavik, R. Schneider, Provenance of present-day eolian dust collected off NW Africa. *J. Geophys. Res.* **110**, D04202 (2005).
25. R. Tjallingii, M. Claussen, J.-B. W. Stuut, J. Fohlmeister, A. Jahn, T. Bickert, F. Lamy, U. Röhl, Coherent high- and low-latitude control of the northwest African hydrological balance. *Nat. Geosci.* **1**, 670–675 (2008).
26. K. M. Yarincik, R. W. Murray, L. C. Peterson, Climatically sensitive eolian and hemipelagic deposition in the Cariaco Basin, Venezuela, over the past 578,000 years: Results from Al/Ti and K/Al. *Paleoceanography* **15**, 210–228 (2000).
27. J. M. Prospero, Long-term measurements of the transport of African mineral dust to the southeastern United States: Implications for regional air quality. *J. Geophys. Res. Atmos.* **104**, 15917–15927 (1999).
28. M. R. Boardman, A. C. Neumann, Sources of periplatform carbonates: Northwest Providence Channel, Bahamas. *J. Sediment. Res.* **54**, 1110–1123 (1984).
29. F. E. Grousset, M. Parra, A. Bory, P. Martinez, P. Bertrand, G. Shimmield, R. M. Ellam, Saharan wind regimes traced by the Sr–Nd isotopic composition of subtropical Atlantic Sediments: Last Glacial Maximum vs today. *Quat. Sci. Rev.* **17**, 395–409 (1998).
30. M. Yoshioka, N. M. Mahowald, A. J. Conley, W. D. Collins, D. W. Fillmore, C. S. Zender, D. B. Coleman, Impact of desert dust radiative forcing on Sahel precipitation: Relative importance of dust compared to sea surface temperature variations, vegetation changes, and greenhouse gas warming. *J. Clim.* **20**, 1445–1467 (2007).
31. M. P. Marcella, E. A. B. Eltahir, The role of mineral aerosols in shaping the regional climate of West Africa. *J. Geophys. Res. Atmos.* **119**, 5806–5822 (2014).
32. F. Solmon, M. Mallet, N. Elguindi, F. Giorgi, A. Zakey, A. Konaré, Dust aerosol impact on regional precipitation over western Africa, mechanisms and sensitivity to absorption properties. *Geophys. Res. Lett.* **35**, L24705 (2008).
33. T. Yuan, L. Oreopoulos, M. Zelinka, H. Yu, J. R. Norris, M. Chin, S. Platnick, K. Meyer, Positive low cloud and dust feedbacks amplify Tropical North Atlantic multidecadal oscillation. *Geophys. Res. Lett.* **43**, 1349–1356 (2016).
34. L. I. Bradtmiller, D. McGee, M. Awalt, J. Evers, H. Yerxa, C. W. Kinsley, P. B. deMenocal, Changes in biological productivity along the northwest African margin over the past 20,000 years. *Paleoceanography* **31**, 185–202 (2016).
35. J. M. Prospero, I. Olmez, M. Ames, Al and Fe in PM 2.5 and PM 10 suspended particles in South-Central Florida: The impact of the long range transport of African mineral dust. *Water Air Soil Pollut.* **125**, 291–317 (2001).
36. J. M. Prospero, W. M. Landing, M. Schulz, African dust deposition to Florida: Temporal and spatial variability and comparisons to models. *J. Geophys. Res. Atmos.* **115**, D13304 (2010).
37. M. R. Boardman, R. F. McCartney, M. R. Eaton, Bahamian paleosols: Origin, relation to paleoclimate, and stratigraphic significance. *Geol. Soc. Am. Spec. Pap.* **300**, 33–49 (1995).
38. E. A. Bettis III, D. R. Muhs, H. M. Roberts, A. G. Wintle, Last Glacial loess in the conterminous USA. *Quat. Sci. Rev.* **22**, 1907–1946 (2003).
39. C. I. Measures, W. M. Landing, M. T. Brown, C. S. Buck, High-resolution Al and Fe data from the Atlantic Ocean CLIVAR-CO_2 Repeat Hydrography A16N transect: Extensive linkages between atmospheric dust and upper ocean geochemistry. *Global Biogeochem. Cycles* **22**, GB1005 (2008).
40. Y.-T. Hsieh, G. M. Henderson, A. L. Thomas, Combining seawater ^{232}Th and ^{230}Th concentrations to determine dust fluxes to the surface ocean. *Earth Planet. Sci. Lett.* **312**, 280–290 (2011).

41. S. R. Taylor, S. M. McLennan, *The Continental Crust: Its Composition and Evolution* (Blackwell Scientific Publications, 1985).
42. J. M. Prospero, R. T. Nees, M. Uematsu, Deposition rate of particulate and dissolved aluminum derived from Saharan dust in precipitation at Miami, Florida. *J. Geophys. Res. Atmos.* **92**, 14723–14731 (1987).
43. W. M. Landing, J. J. Perry Jr., J. L. Guentzel, G. A. Gill, C. D. Pollman, Relationships between the atmospheric deposition of trace elements, major ions, and mercury in Florida: The FAMS project (1992–1993). *Water Air Soil Pollut.* **80**, 343–352 (1995).
44. R. Francois, M. Frank, M. M. R. van der Loeff, M. P. Bacon, ^{230}Th normalization: An essential tool for interpreting sedimentary fluxes during the late Quaternary. *Paleoceanography* **19**, PA1018 (2004).
45. D. McGee, G. Winckler, A. Borunda, S. Serno, R. F. Anderson, C. Recasens, A. Bory, D. Gaiero, S. L. Jaccard, M. Kaplan, J. F. McManus, M. Revel, Y. Sun, Tracking eolian dust with helium and thorium: Impacts of grain size and provenance. *Geochim. Cosmochim. Acta* **175**, 47–67 (2016).
46. N. C. Slowey, G. M. Henderson, Radiocarbon ages constraints on the origin and shedding of bank-top sediment in the Bahamas during the Holocene. *Aquat. Geochem.* **17**, 419–429 (2011).
47. G. M. Henderson, F. N. Lindsay, N. C. Slowey, Variation in bioturbation with water depth on marine slopes: A study on the Little Bahamas Bank. *Mar. Geol.* **160**, 105–118 (1999).
48. W. H. Berger, G. R. Heath, Vertical mixing in pelagic sediments. *J. Mar. Res.* **26**, 134–143 (1968).
49. R. Francois, M. P. Bacon, Variations in terrigenous input into the deep equatorial Atlantic during the past 24,000 years. *Science* **251**, 1473–1476 (1991).
50. J. A. Arbuszewski, P. B. deMenocal, C. Cléroux, L. Bradtmiller, A. Mix, Meridional shifts of the Atlantic intertropical convergence zone since the Last Glacial Maximum. *Nat. Geosci.* **6**, 959–962 (2013).
51. S. Albani, N. M. Mahowald, A. T. Perry, R. A. Scanza, C. S. Zender, N. G. Heavens, V. Maggi, J. F. Kok, B. L. Otto-Bliesner, Improved dust representation in the Community Atmosphere Model. *J. Adv. Model. Earth Syst.* **6**, 541–570 (2014).
52. A. T. Evan, C. Flamant, S. Fiedler, O. Doherty, An analysis of aeolian dust in climate models. *Geophys. Res. Lett.* **41**, 5996–6001 (2014).
53. N. Mahowald, S. Albani, J. F. Kok, S. Engelstaeder, R. Scanza, D. S. Ward, M. G. Flanner, The size distribution of desert dust aerosols and its impact on the Earth system. *Aeolian Res.* **15**, 53–71 (2014).
54. A. Donohoe, J. Marshall, D. Ferreira, D. McGee, The relationship between ITCZ location and cross-equatorial atmospheric heat transport: From the seasonal cycle to the Last Glacial Maximum. *J. Clim.* **26**, 3597–3618 (2013).
55. D. McGee, A. Donohoe, J. Marshall, D. Ferreira, Changes in ITCZ location and cross-equatorial heat transport at the Last Glacial Maximum, Heinrich Stadial 1, and the mid-Holocene. *Earth Planet. Sci. Lett.* **390**, 69–79 (2014).
56. W. Wang, A. T. Evan, C. Flamant, C. Lavaysse, On the decadal scale correlation between African dust and Sahel rainfall: The role of Saharan heat low-forced winds. *Sci. Adv.* **1**, e1500646 (2015).
57. P. K. Swart, A. M. Oehlert, G. J. Mackenzie, G. P. Eberli, J. J. G. Reijmer, The fertilization of the Bahamas by Saharan dust: A trigger for carbonate precipitation? *Geology* **42**, 671–674 (2014).
58. E. A. Shinn, G. W. Smith, J. M. Prospero, P. Betzer, M. L. Hayes, V. Garrison, R. T. Barber, African dust and the demise of Caribbean coral reefs. *Geophys. Res. Lett.* **27**, 3029–3032 (2000).
59. H. Ren, D. M. Sigman, A. N. Meckler, B. Plessen, R. S. Robinson, Y. Rosenthal, G. H. Haug, Foraminiferal isotope evidence of reduced nitrogen fixation in the Ice Age Atlantic Ocean. *Science* **323**, 244–248 (2009).
60. A. N. Meckler, H. Ren, D. M. Sigman, N. Gruber, B. Plessen, C. J. Schubert, G. H. Haug, Deglacial nitrogen isotope changes in the Gulf of Mexico: Evidence from bulk sedimentary and foraminifera-bound nitrogen in Orca Basin sediments. *Paleoceanography* **26**, PA4216 (2011).
61. B. A. Ward, S. Dutkiewicz, C. M. Moore, M. J. Follows, Iron, phosphorus, and nitrogen supply ratios define the biogeography of nitrogen fixation. *Limnol. Oceanogr.* **58**, 2059–2075 (2013).
62. M. Straub, D. M. Sigman, H. Ren, A. Martínez-García, A. N. Meckler, M. P. Hain, G. H. Haug, Changes in North Atlantic nitrogen fixation controlled by ocean circulation. *Nature* **501**, 200–203 (2013).
63. J. E. Kutzbach, Z. Liu, Response of the African Monsoon to orbital forcing and ocean feedbacks in the Middle Holocene. *Science* **278**, 440–443 (1997).
64. A. Ganopolski, C. Kubatzki, M. Claussen, V. Brovkin, V. Petoukhov, The influence of vegetation-atmosphere-ocean interaction on climate during the Mid-Holocene. *Science* **280**, 1916–1919 (1998).
65. J. Perlwitz, I. Tegen, R. L. Miller, Interactive soil dust aerosol model in the GISS GCM: 1. Sensitivity of the soil dust cycle to radiative properties of soil dust aerosols. *J. Geophys. Res. Atmos.* **106**, 18167–18192 (2001).
66. R. Li, Q.-L. Min, L. C. Harrison, A case study: The indirect aerosol effects of mineral dust on warm clouds. *J. Atmos. Sci.* **67**, 805–816 (2010.
67. D. Rosenfeld, Y. Rudich, R. Lahav, Desert dust suppressing precipitation: A possible desertification feedback loop. *Proc. Natl. Acad. Sci. U.S.A.* **98**, 5975–5980 (2001).
68. Y. Gu, K. N. Liou, J. H. Jiang, H. Su, X. Liu, Dust aerosol impact on North Africa climate: A GCM investigation of aerosol-cloud-radiation interactions using A-Train satellite data. *Atmos. Chem. Phys.* **12**, 1667–1679 (2012).
69. O. A. Choobari, P. Zawar-Reza, A. Sturman, The global distribution of mineral dust and its impacts on the climate system: A review. *Atmos. Res.* **138**, 152–165 (2014).
70. Q.-L. Min, R. Li, B. Lin, E. Joseph, S. Wang, Y. Hu, V. Morris, F. Chang, Evidence of mineral dust altering cloud microphysics and precipitation. *Atmos. Chem. Phys. Discuss.* **8**, 18893–18910 (2008).
71. S. Albani, N. M. Mahowald, G. Winckler, R. F. Anderson, L. I. Bradtmiller, B. Delmonte, R. François, M. Goman, N. G. Heavens, P. P. Hesse, S. A. Hovan, S. G. Kang, K. E. Kohfeld, H. Lu, V. Maggi, J. A. Mason, P. A. Mayewski, D. McGee, X. Miao, B. L. Otto-Bliesner, A. T. Perry, A. Pourmand, H. M. Roberts, N. Rosenbloom, T. Stevens, J. Sun, Twelve thousand years of dust: The Holocene global dust cycle constrained by natural archives. *Clim. Past* **11**, 869–903 (2015).
72. S. Egerer, M. Claussen, C. Reick, T. Stanelle, The link between marine sediment records and changes in Holocene Saharan landscape: Simulating the dust cycle. *Clim. Past* **12**, 1009–1027 (2016).
73. N. Huneeus, M. Schulz, Y. Balkanski, J. Griesfeller, J. Prospero, S. Kinne, S. Bauer, O. Boucher, M. Chin, F. Dentener, T. Diehl, R. Easter, D. Fillmore, S. Ghan, P. Ginoux, A. Grini, L. Horowitz, D. Koch, M. C. Krol, W. Landing, X. Liu, N. Mahowald, R. Miller, J.-J. Morcrette, G. Myhre, J. Penner, J. Perlwitz, P. Stier, T. Takemura, C. S. Zender, Global dust model intercomparison in AeroCom phase I. *Atmos. Chem. Phys.* **11**, 7781–7816 (2011).
74. R. B. Neale, J. H. Richter, A. J. Conley, S. Park, P. H. Lauritzen, A. Gettelman, D. L. Williamson, *Description of the NCAR Community Atmosphere Model (CAM 4.0)* (National Center for Atmospheric Research, 2010).
75. P. R. Gent, G. Danabasoglu, L. J. Donner, M. M. Holland, E. C. Hunke, S. R. Jayne, D. M. Lawrence, R. B. Neale, P. J. Rasch, M. Vertenstein, P. H. Worley, Z.-L. Yang, M. Zhang, The Community Climate System Model Version 4. *J. Clim.* **24**, 4973–4991 (2011).
76. R. Kahn, P. Banerjee, D. McDonald, Sensitivity of multiangle imaging to natural mixtures of aerosols over ocean. *J. Geophys. Res.* **106**, 18219–18238 (2001).
77. J. Laskar, A. Fienga, M. Gastineau, H. Manche, La2010: A new orbital solution for the long-term motion of the Earth. *Astron. Astrophys.* **532**, A89 (2011).
78. S. J. Burns, A. C. Neumann, Pelagic sedimentation on an inactive gullied slope, Northwest Providence Channel, Bahamas. *Mar. Geol.* **77**, 277–286 (1987).
79. J. D. Milliman, D. Freile, R. P. Steilin, R. J. Wilber, Great Bahama Bank aragonitic muds: Mostly inorganically precipitated, mostly exported. *J. Sediment. Petrol.* **63**, 589–595 (1993).
80. N. C. Slowey, W. B. Curry, Glacial-interglacial differences in circulation and carbon cycling within the upper western North Atlantic. *Paleoceanography* **10**, 715–732 (1995).
81. R. E. Came, D. W. Oppo, W. B. Curry, Atlantic Ocean circulation during the Younger Dryas: Insights from a new Cd/Ca record from the western subtropical South Atlantic. *Paleoceanography* **18**, 1086 (2003).
82. R. E. Came, D. W. Oppo, W. B. Curry, J. Lynch-Stieglitz, Deglacial variability in the surface return flow of the Atlantic meridional overturning circulation. *Paleoceanography* **23**, PA1217 (2008).
83. P. J. Reimer, E. Bard, A. Bayliss, J. W. Beck, P. G. Blackwell, C. B. Ramsey, C. E. Buck, H. Cheng, R. L. Edwards, M. Friedrich, P. M. Grootes, T. P. Guilderson, H. Haflidason, I. Hajdas, C. Hatté, T. J. Heaton, D. L. Hoffmann, A. G. Hogg, K. A. Hughen, K. F. Kaiser, B. Kromer, S. W. Manning, M. Niu, R. W. Reimer, D. A. Richards, E. M. Scott, J. R. Southon, R. A. Staff, C. S. M. Turney, J. van der Plich, IntCal13 and Marine13 radiocarbon age calibration curves 0–50,000 years cal BP. *Radiocarbon* **55**, 1869–1887 (2013).
84. C. B. Ramsey, Deposition models for chronological records. *Quat. Sci. Rev.* **27**, 42–60 (2008).
85. N. C. Slowey, R. J. Wilber, G. A. Haddad, G. M. Henderson, Glacial-to-Holocene sedimentation on the western slope of Great Bahama Bank. *Mar. Geol.* **185**, 165–176 (2002).
86. R. Francois, M. Frank, M. R. van der Loeff, M. P. Bacon, W. Geibert, S. Kienast, R. F. Anderson, L. Bradtmiller, Z. Chase, G. Henderson, F. Marcantonio, S. E. Allen, Comment on "Do geochemical estimates of sediment focusing pass the sediment test in the equatorial Pacific?" by M. Lyle et al. *Paleoceanography* **22**, PA1216 (2007).
87. G. M. Henderson, C. Heinze, R. F. Anderson, A. M. E. Winguth, Global distribution of the ^{230}Th flux to ocean sediments constrained by GCM modelling. *Deep Sea Res. Part I Oceanogr. Res. Pap.* **46**, 1861–1893 (1999).
88. C. T. Hayes, R. F. Anderson, M. Q. Fleisher, K.-F. Huang, L. F. Robinson, Y. Lu, H. Cheng, R. L. Edwards, S. B. Moran, ^{230}Th and ^{231}Pa on GEOTRACES GA03, the U.S. GEOTRACES North Atlantic transect, and implications for modern and paleoceanographic chemical fluxes. *Deep Sea Res. Part II Top. Stud. Oceanogr.* **116**, 29–41 (2015).

89. R. F. Anderson, M. Q. Fleisher, Y. Lao, Glacial–interglacial variability in the delivery of dust to the central equatorial Pacific Ocean. *Earth Planet. Sci. Lett.* **242**, 406–414 (2006).
90. H. Snoeckx, D. K. Rea, Dry bulk density and $CaCO_3$ relationships in upper Quaternary sediments of the eastern equatorial Pacific. *Mar. Geol.* **120**, 327–333 (1994).
91. M. Ewing, J. I. Ewing, M. Talwani, Sediment distribution in the oceans: The Mid-Atlantic Ridge. *Bull. Geol. Soc. Am.* **75**, 17–35 (1964).
92. D. McGee, F. Marcantonio, J. F. McManus, G. Winckler, The response of excess ^{230}Th and extraterrestrial ^{3}He to sediment redistribution at the Blake Ridge, western North Atlantic. *Earth Planet. Sci. Lett.* **299**, 138–149 (2010).
93. J. Thomson, S. Colley, R. Anderson, G. T. Cook, A. B. MacKenzie, D. D. Harkness, Holocene sediment fluxes in the northeast Atlantic from $^{230}Th_{excess}$ and radiocarbon measurements. *Paleoceanography* **8**, 631–650 (1993).
94. J. Thomson, D. R. H. Green, P. van Calsteren, T. O. Richter, T. C. E. van Weering, Holocene sediment deposition on a NE Atlantic transect including Feni Drift quantified by radiocarbon and $^{230}Th_{excess}$ methods. *Earth Planet. Sci. Lett.* **242**, 170–185 (2006).

Acknowledgments: We thank W. Curry and the Lamont-Doherty Core Repository for providing access to these cores. We thank S. Mallick and A. Saal at Brown University and T. Ireland and A. Dunlea at Boston University for facilitating mass spectrometric measurements, Y.-T. Hsieh for providing key assistance with method development, and Z. Norberg for assisting with sample preparation. We thank S. Albani, L. Murphy, and N. Mahowald for helpful input about GCM experiments and dust optical parameters and R. F. Anderson and two anonymous reviewers for thoughtful comments that improved the manuscript. **Funding:** This study was supported, in part, by NSF awards OCE-1030784 (to D.M. and P.B.d.) and OCE-09277247 (to P.B.d.); NASA grant NN14AP38G (to C. Heald, Massachusetts Institute of Technology), which supports D.A.R.; and the Columbia University Center for Climate and Life. A.F. is supported by the NSF grant AGS-1116885 and the National Oceanic and Atmospheric Administration (NOAA) grant NA14OAR4310277. S.H. is supported by the NASA Earth and Space Sciences Fellowship. We also acknowledge computational support from the NSF/NCAR Yellowstone Supercomputing Center and the Yale University High Performance Computing Center. Portions of this material are based on work supported while R.W.M. was serving at the NSF. **Author contributions:** D.M. conceived the study. R.H.W., C.W.K., I.T., and D.M. prepared samples and collected U-Th data. I.T., C.W.K., and R.W.M. collected trace element data. P.B.d. contributed samples and ^{14}C ages for core VM20-234. S.H. and A.F. designed, conducted, and analyzed GCM experiments. D.M. and R.H.W. wrote the manuscript with input and figures from D.A.R. and S.H. All authors edited the manuscript. **Competing interests:** The authors declare that they have no competing interests. **Data and materials availability:** All geochemical data are provided in the Supplementary Materials and are archived at the NOAA World Data Center for Paleoclimatology. Additional data related to this paper may be requested from the authors.

Submitted 29 February 2016
Accepted 20 October 2016
Published 23 November 2016
10.1126/sciadv.1600445

Citation: R. H. Williams, D. McGee, C. W. Kinsley, D. A. Ridley, S. Hu, A. Fedorov, I. Tal, R. W. Murray, P. B. deMenocal, Glacial to Holocene changes in trans-Atlantic Saharan dust transport and dust-climate feedbacks. *Sci. Adv.* **2**, e1600445 (2016).

ScienceAdvances
AAAS

Glacial to Holocene changes in trans-Atlantic Saharan dust transport and dust-climate feedbacks

Ross H. Williams, David McGee, Christopher W. Kinsley, David A. Ridley, Shineng Hu, Alexey Fedorov, Irit Tal, Richard W. Murray and Peter B. deMenocal (November 23, 2016)

Sci Adv 2016, 2:.
doi: 10.1126/sciadv.1600445